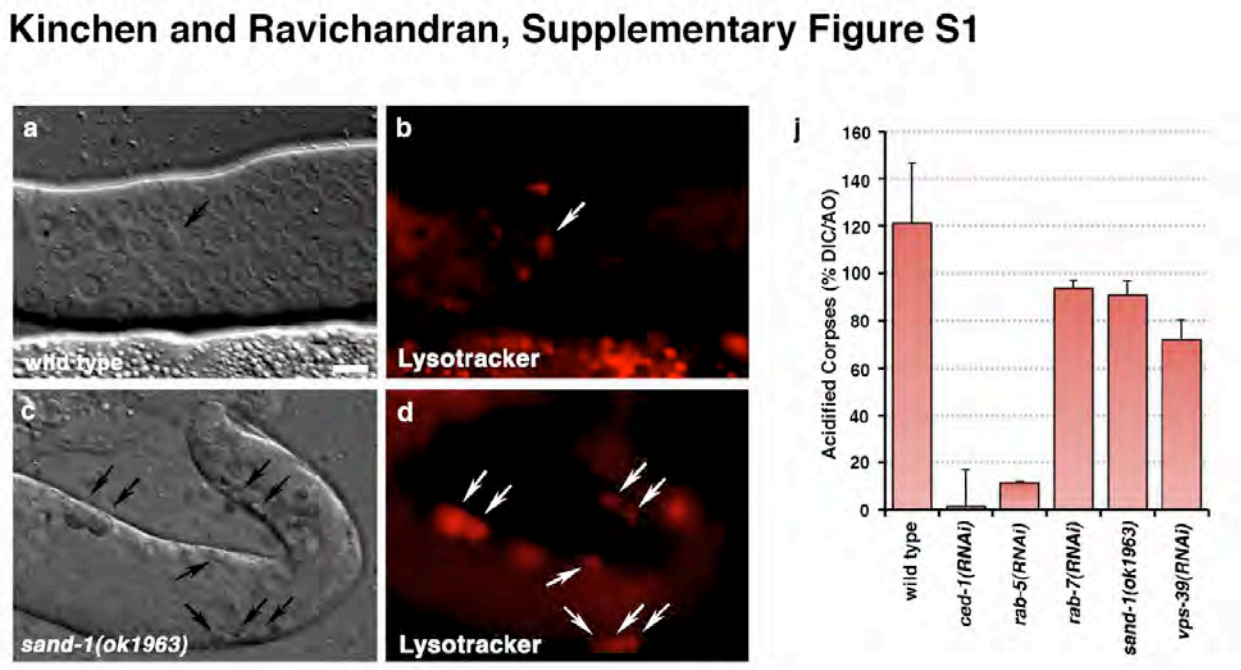

Supplementary Figure S1. Apoptotic cell corpses in *sand-1(ok1963*) mutants are arrested at a late stage of corpse removal.

(**a**-**d**) *sand-1(lf)* does not block phagosome acidification. Acridine orange and LysoTracker Red stains are frequently used to stain internalized apoptotic cells within acidic phagolysosome structures; onset of staining appears to be soon after recruitment of RAB-5 to the phagosome. In *sand-1(ok1963)* mutant worms the majority of refractile apoptotic cells continued to stain with acridine orange and Lysotracker red (**c**, **d**), similar to wild-type worms (**a**, **b**). Bright field represents DIC micrographs.

(**e**) Quantitation of acridine orange (AO) staining corpses of 12h post L4/adult molt gonads. Data shown in (**e**) represents number of AO positive bodies divided by number of refractile cell corpses ± s.e.m. In *wild-type* worms, we frequently see large AO-posititve, non-refractile structures within the gonad which represent apoptotic cells at late stages of degradation that have lost refractility giving ratios >100%. *n* is shown in Table 1.

Kinchen and Ravichandran, Supplementary Figure S2

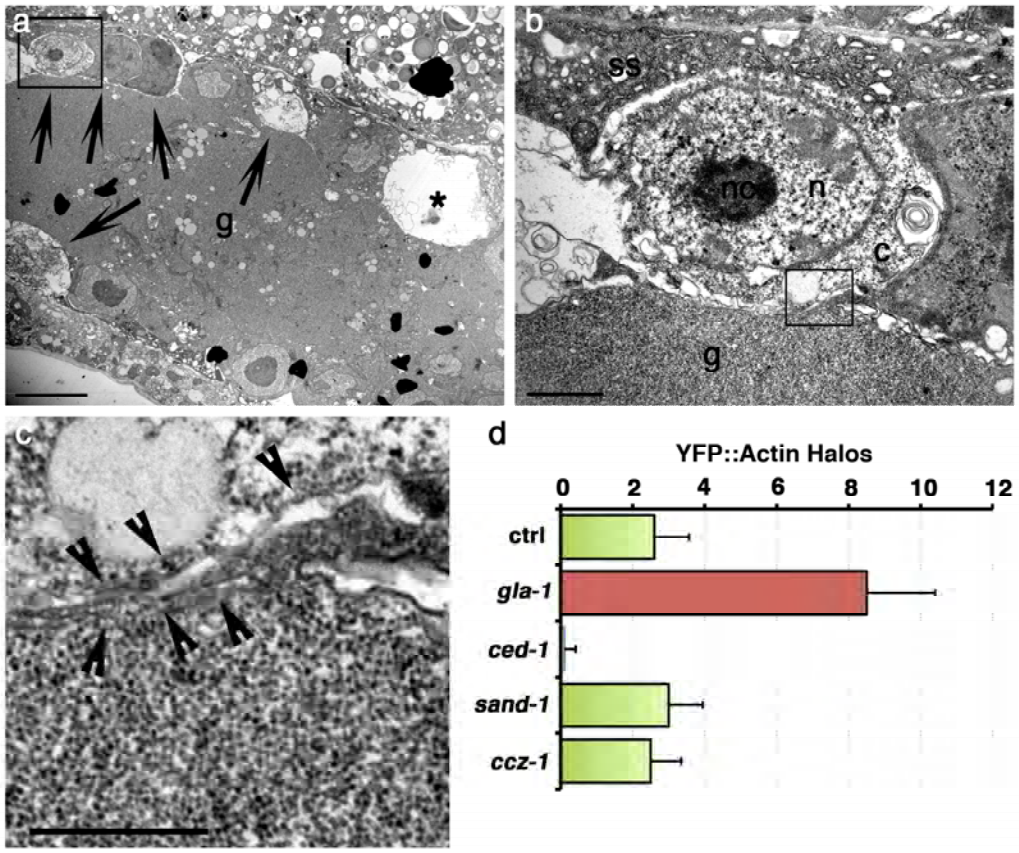

Supplementary Figure S2. Apoptotic cell corpses are engulfed and arrested at a late stage of degradation in *sand-1* and *ccz-1* mutant worms.

(**a**-**c**) *sand-1(ok1963*) mutant worms were fixed in paraformaldehyde, mounted in Epon, then sectioned and analyzed at the ultrastructural level for defects in apoptotic cell removal. The germ line of *sand-1(ok1963)* mutant worms was filled with engulfed apoptotic cells, with many phagosomes containing multiple cell corpses (**a**, arrows). Asterisk marks an enlarged lysosome structure that may have held apoptotic cell(s) at one time. A close-up of boxed area in (**a**) is shown in (**b)**. At least two sets of membrane are present surrounding the apoptotic cell (higher mag, **c**).

(**d**) Actin reorganization during corpse internalization appears normal in *sand-1(RNAi)* and *ccz-1(RNAi)*; in contrast, *ced-1(RNAi)* worms show defects in corpse internalization (decreased numbers of YFP::Actin halos). Enhanced induction of apoptosis was not detected in *sand-1(RNAi)* or *ccz-1(RNAi)* animals (compare to *gla-1*, which shows increased numbers of YFP::Actin halos related to increased basal germ cell apoptosis).

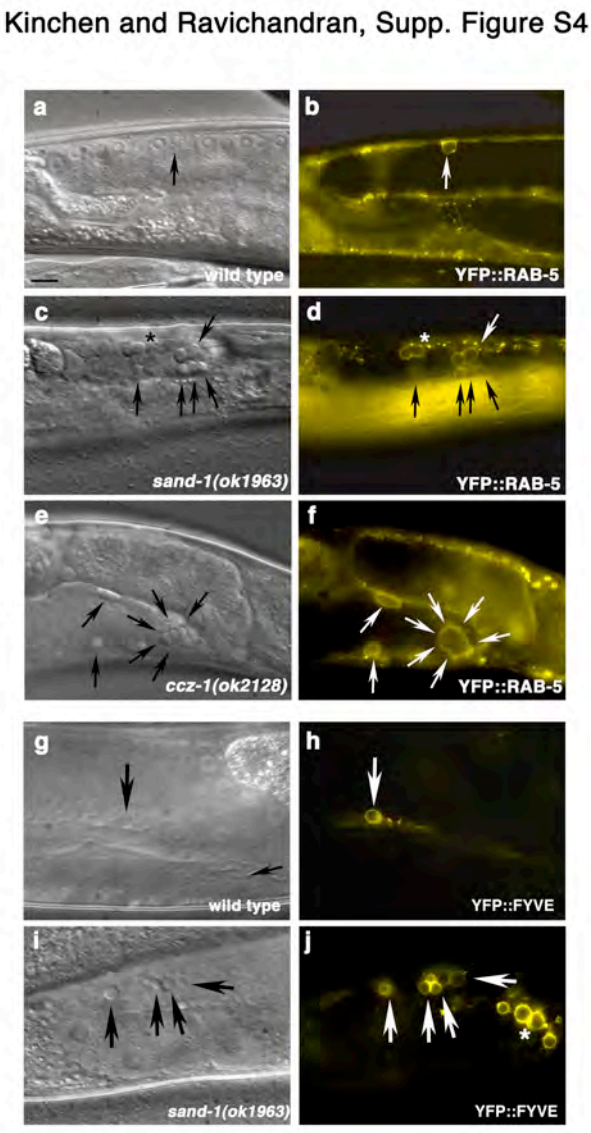

Supplementary Figure S3. Widefield images of confocal micrographs of corpses in RAB-5(+) or 2xFYVE(+) phagosomes from Fig. 2

Size bar, 10μm. Widefield images showing RAB-5 (a-) or 2xFYVE () phagosomes in various mutant backgrounds. This data mirrors that in Fig. 2 but is shown because DIC optics on confocal microscopes do not adequately show refractility of apoptotic cells.

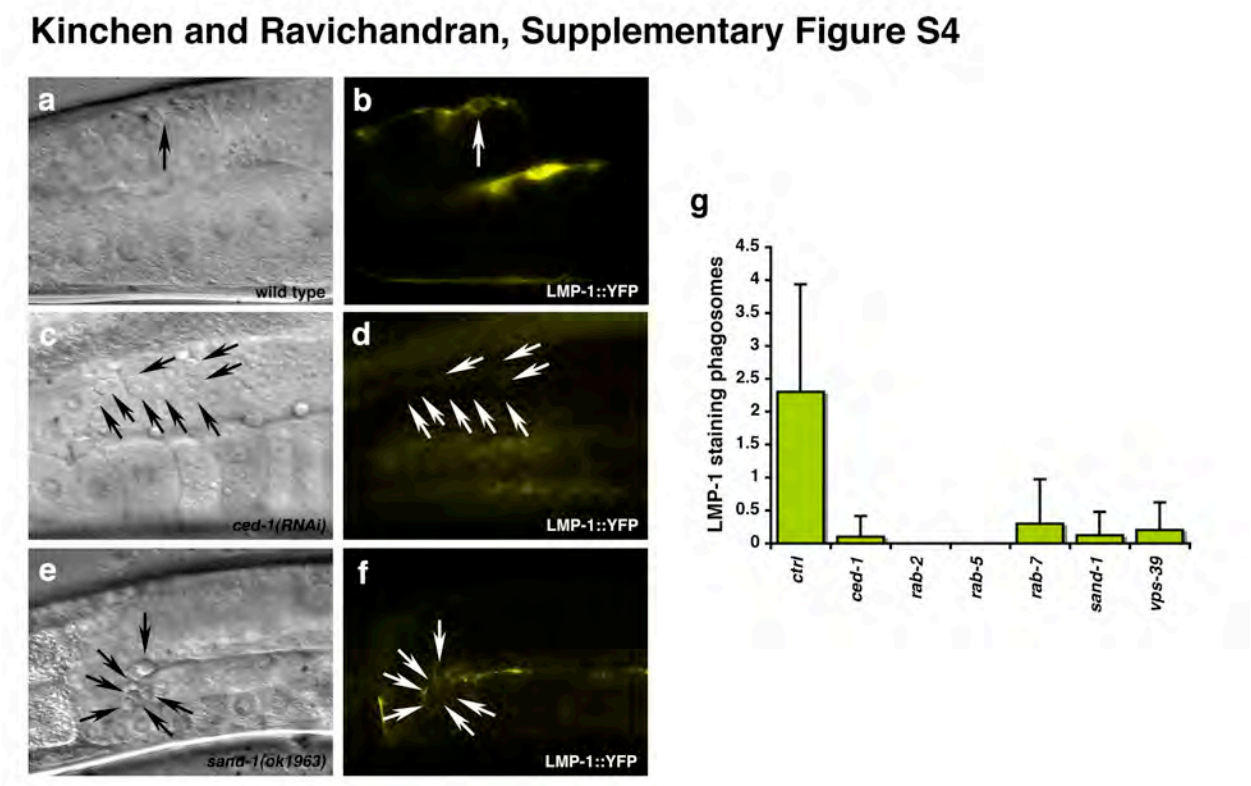

Supplementary Figure S4. Phagosome-lysosome fusion is decreased in *sand-1(ok1963)* mutant worms.

(**a**-**f**) Phagosome-lysosome fusion was measured by recruitment of LMP-1::YFP (LAMP-1) to the phagosome. Compared to wild-type worms (**a**, **b**), apoptotic cells in *ced-1(RNAi)* (**c**, **d**) which depletes the *ced-1*,phagocytic receptor) or *sand-1(ok1963)* mutant worms (**e**, **f**) show decreased levels of LMP-1::YFP to the phagosome surface. Data shown represents mean ± s.d.

(**g**) Quantitation of data presented in (**a**-**f**).

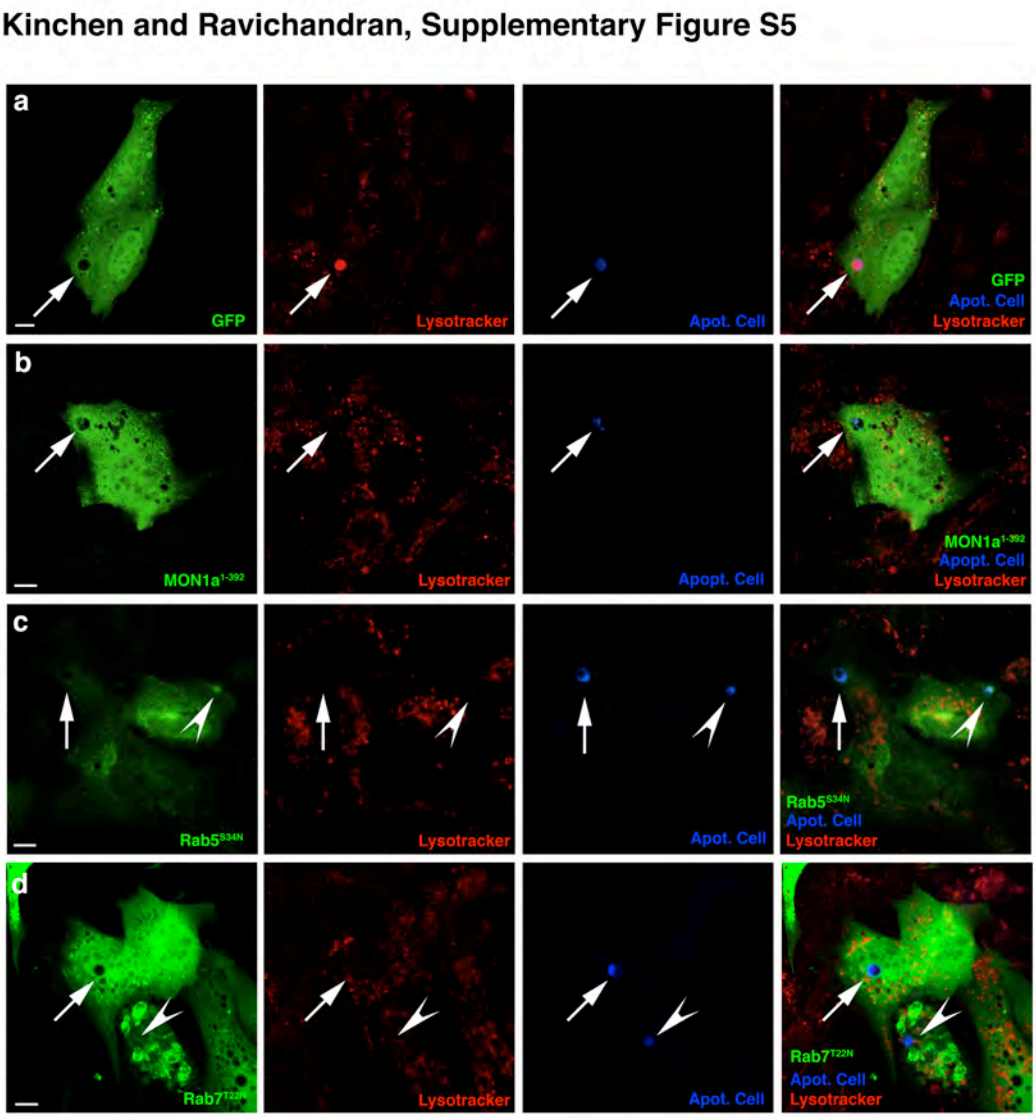

Supplementary Figure S5. Individual Panels from colocalization in Fig. 4, a-e

Size bar, 10μm. Arrows point to apoptotic cell (blue) or co-localization between apoptotic cell and Lysotracker Red (red) within NIH/T3T cells used as phagocytes. The ratio of apoptotic thymocytes used was 0.5 per phagocyte, as this provided optimal conditions for measuring degradation in this system. Transfected protein is shown in green.

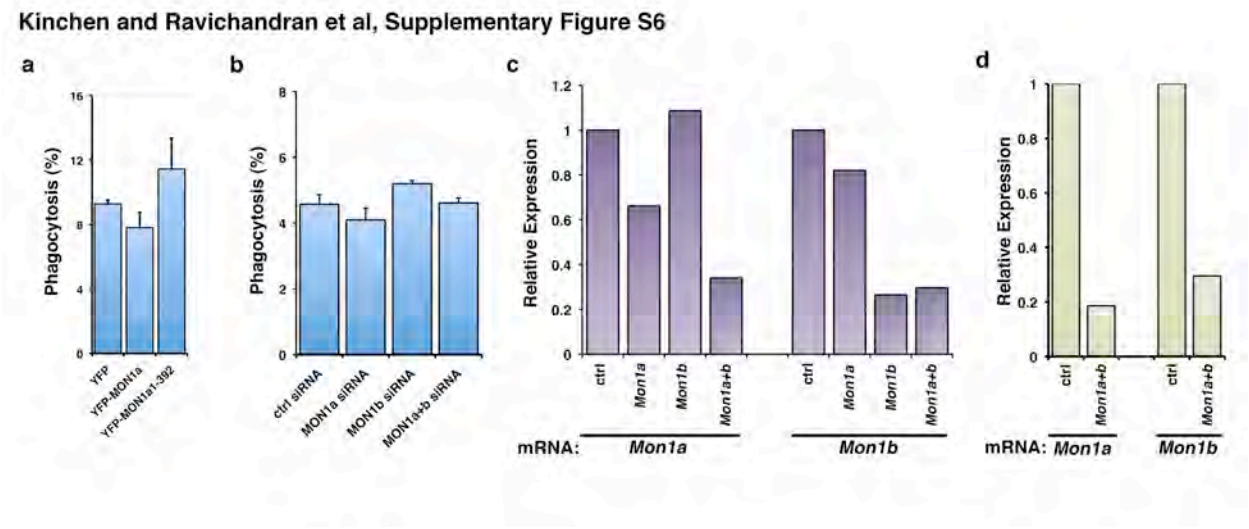

Supplementary Figure S6. Inhibition of Mon1 function does not cause phagocytic defects.

(**a**, **b**) Phagocytes were transfected with the indicated constructs or electroporated with the indicated siRNAs and incubated for 18 or 48h, respectively. These cells were then incubated with apoptotic SCI cells for 2h. Phagocytes were then trypsinized and analyzed by flow cytometry to quantitate the percentage of cells engulfing apoptotic cells. No significant defect in apoptotic cell internalization *per se* was detected in NIH/3T3 cells transfected either with a MON1a$^{1-392}$ truncation (**a**) or electroporated with siRNA targeting *Mon1a, Mon1b* or *Mon1a* and *Mon1b* (**b**). Data shown as mean ± s.d; one representative experiment (of at least three) is shown.

(**c**) Quantitative RT-PCR (Q-RT-PCR) was used to determine the relative levels of *Mon1a* and *Mon1*b (normalized to GAPDH as control) from the RNAi experiment in (**b**).

(**d**) Q-RT-PCR analysis of *Mon1a* and *Mon1b* knockdown from Lysotracker staining experiment shown in Figure 3.

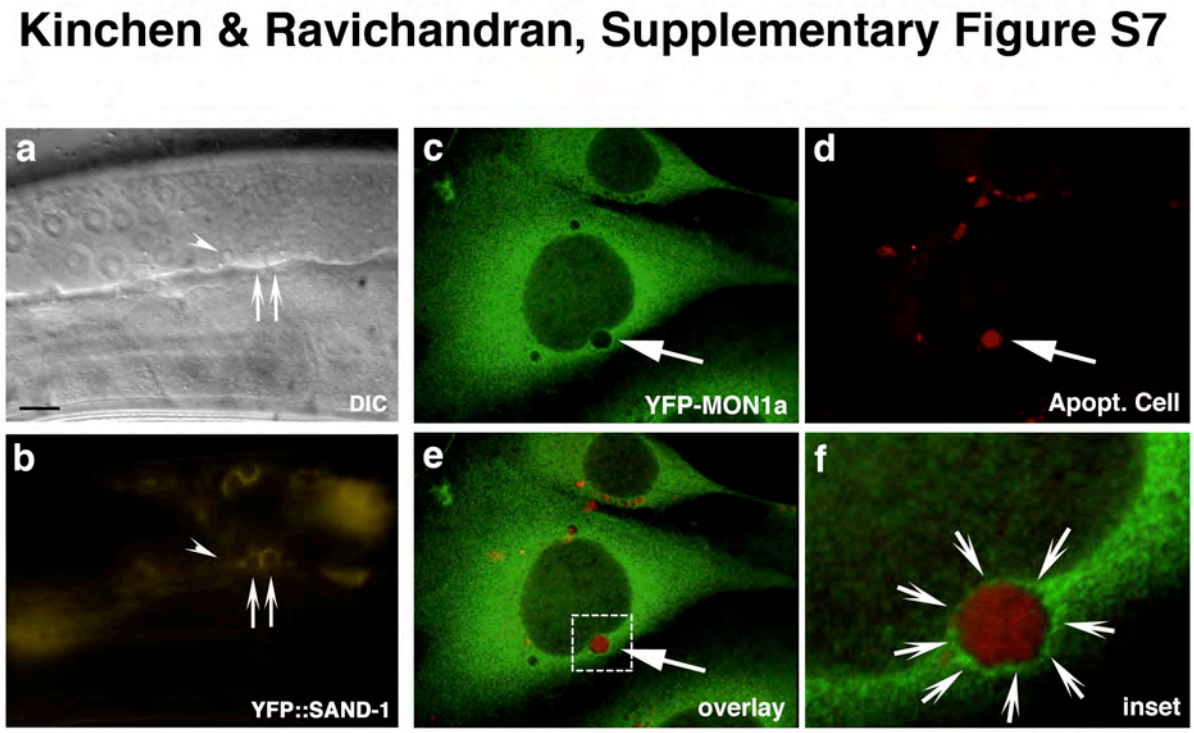

Supplementary Figure S7. YFP::SAND-1 and YFP-Mon1a can localize to phagosomes containing apoptotic cells.

(**a**, **b**) YFP::SAND-1 was expressed under the *ced-1* promoter in the phagocytic sheath cells surrounding the gonad. Arrows point to apoptotic cells (**a**, DIC) or YFP::SAND-1 localization to the phagosome (**b**, YFP::SAND-1).

(**c**-**f**) TMRA-labeled apoptotic thymocytes (**d**) were incubated with NIH/3T3 fibroblasts stably transfected with YFP-Mon1a (**c**, Alexa 488 anti-GFP, green) and the localization of YFP-Mon1a was assessed. Internalized apoptotic cells (arrow) could readily be identified within YFP-Mon1a-positive phagosome structures (**e**, **f**, arrows).

(**g**) Quantitation of data presented in (**a**-**f**).

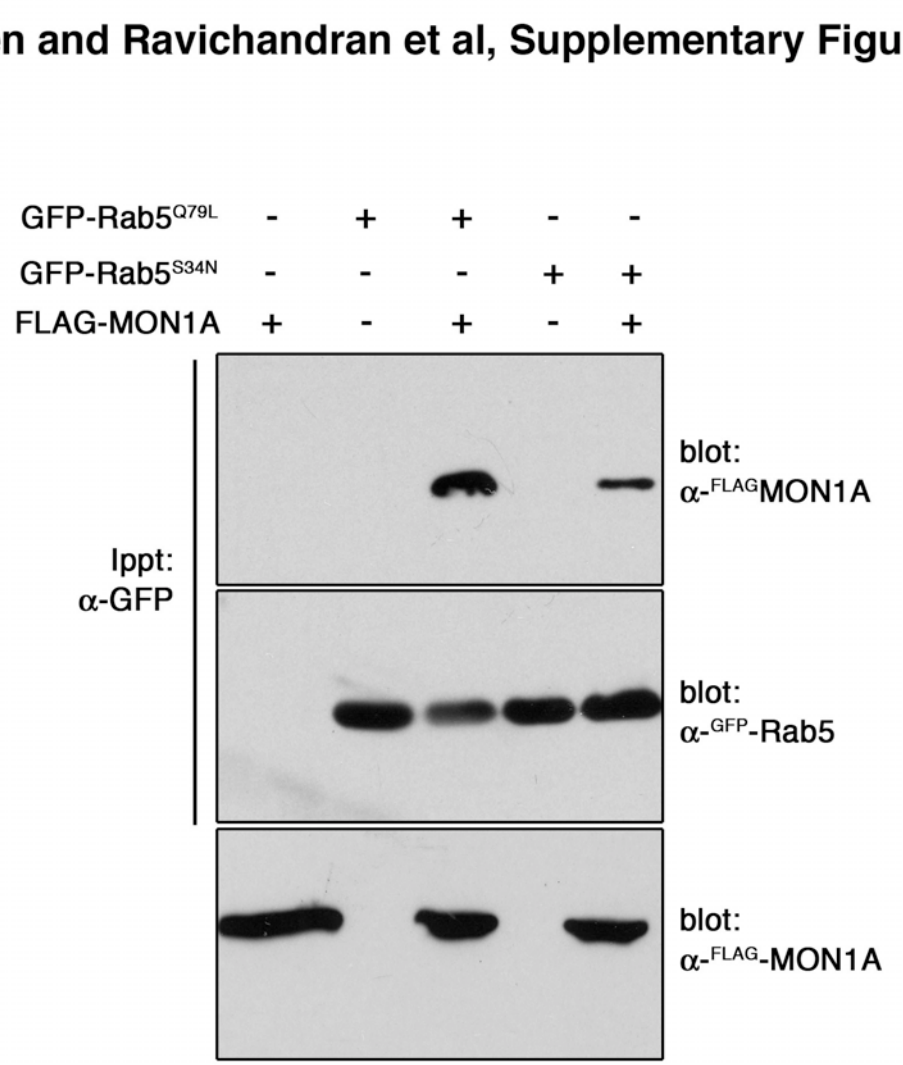

Supplementary Figure S8. Mon1a shows a stronger interaction with $Rab5^{GTP}$ than $Rab5^{GDP}$.

293T cells were transfected with the indicated constructs, treated with lysis buffer containing 5mM $MgCl_2$ and immunoprecipitated with an anti-GFP antibody coupled to sepharose to precipitate GFP-$Rab5^{S34N}$ or GFP-$Rab5^{Q79L}$. After washing, lysates were subjected to immunoblotting with the indicated antibody.

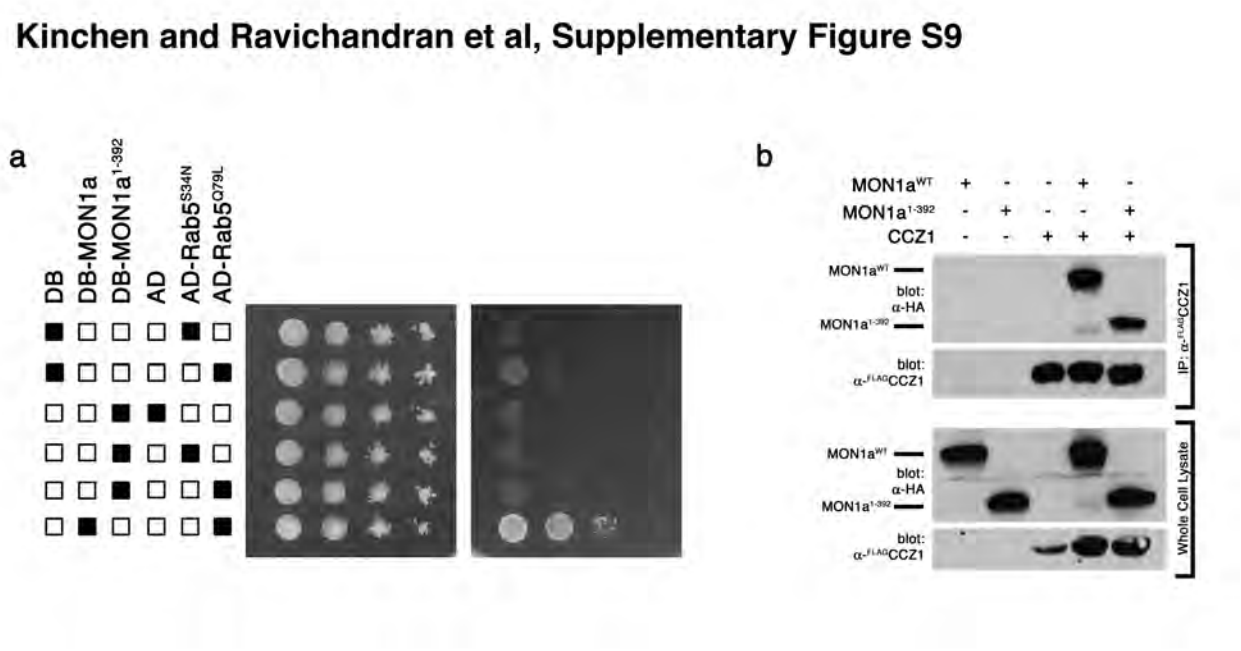

Supplementary Figure S9. Mon1a$^{1-392}$ can interact with CCZ1 but not Rab5^{GTP}.

(**a**) Yeast strain HF7c was transfected with the indicated constructs and assayed for protein interaction by growth on DO –W-L-H + 1mM 3AT (Selective Media). Strains were also plated on DO -W-L (Nonselective Media) to confirm culture viability.

(**b**) 293T cells were transfected with the indicated constructs, lysed in lysis buffer containing 5mM $MgCl_2$ and immunoprecipitated with an anti-FLAG (clone M2) antibody coupled to sepharose. After washing, lysates were subjected to immunoblotting.

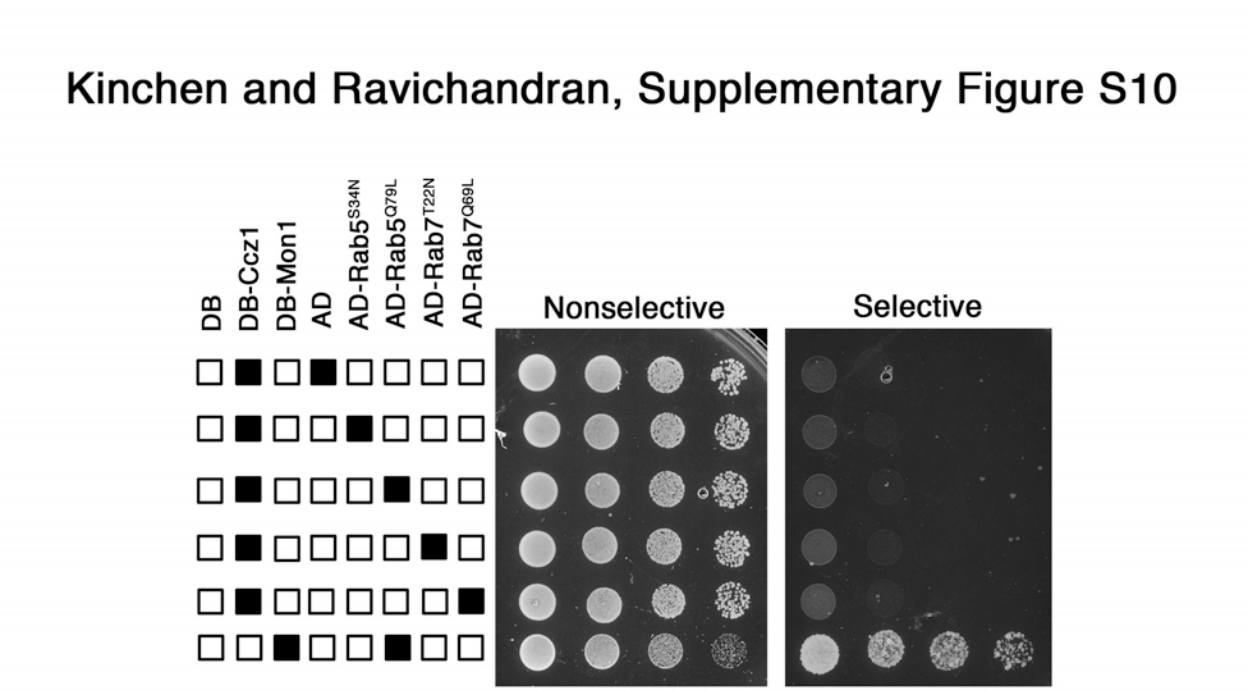

Supplementary Figure S10. CCZ1 does not interact with Rab5 or Rab7 in the yeast two-hybrid.

S. cerevisiae HF7c were transfected with the indicated constructs and assayed for protein interaction by growth on selective medium (DO –Trp-Leu-His +1mM 3AT). Strains were also plated on nonselective media (DO –Trp-Leu) to confirm their viability.

Kinchen & Ravichandran, Suppelmentary Figure S11

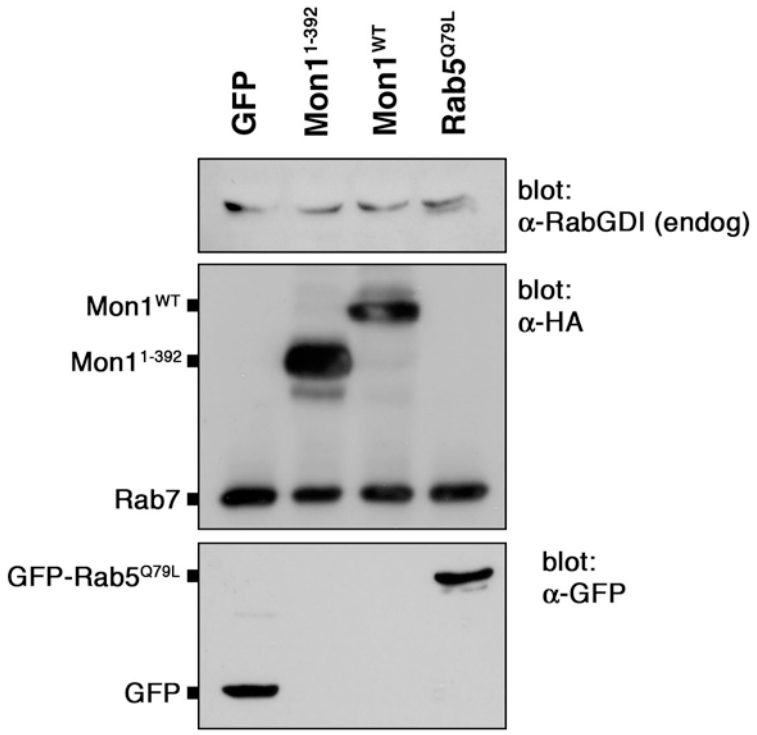

Supplementary Figure S11. Total Cell Lysate for Figure 4, e

293T cells were transfected with the indicated constructs, treated with lysis buffer containing 5mM $MgCl_2$ and immunoprecipitated with an anti-HA antibody coupled to sepharose to precipitate HA-Rab7 complexed to endogenous RabGDI (shown in **Figure 4d**). Western blot shown represents protein expression in total cell lysates.

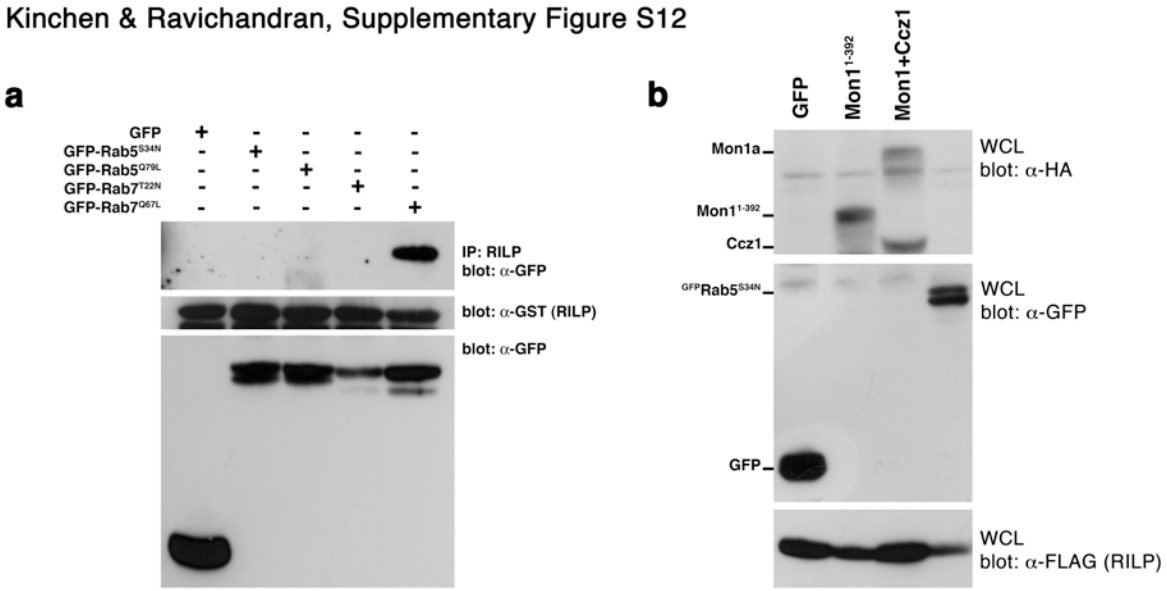

Supplementary Figure S12. RILP binds specifically to active Rab7; Loading Controls for Figure 4e

(**a**) 293T fibroblasts were transiently transfected with constructs encoding active ($Rab5^{Q79L}$, $Rab7^{Q67L}$) or GDP-locked ($Rab5^{S34N}$, $Rab7^{T22N}$) GTPase, lysed and incubated with GST-RILP to precipitate Rab7GTP, which was then assessed by immunoblotting.

(**b**) Protein expression from total cell lysate for immunoprecipitation presented in **Figure 4e**.

Supplementary Table 1. Nematode strains were scored 12-hr post L4/adult molt as described in methods. *n*, number of animals analyzed; data shown represents mean ± s.d.

Supplementary Table S1a. *sand-1* is required for efficient removal of apoptotic cells.

Genotype	Corpse Number	*n*
wild type	2.2 ± 0.8	20
ced-6(n1813)	13.2 ± 2.6	20
sand-1(RNAi)	13.7 ± 2.3	10
sand-1(ok1963)	12.3 ± 2.4	20
ccz-1(RNAi)	11.5 ± 2.9	10
ccz-1(ok2128)	13.2 ± 2.1	13
ced-3(n717)	0.1 ± 0.2	20
ced-3(n717); sand-1(ok1963)	0	20
sand-1(ok1963); vfEx152 [P_{ced-1}::yfp::sand-1(+)]	1.5 ± 1.0	20
sand-1(ok1963); vfIs3 [P_{ced-1}::yfp::sand-1(+)]	1.4 ± 0.8	10
sand-1(ok1963); vfEx187 [P_{ced-1}::yfp::Mon1(+)]	2.5 ± 1.8	10

Table S1b. *sand-1* is not required for phagosome acidification

Genotype	Corpse Number	AO	*n*
wild type	2.1 ± 0.9	2.5 ± 1.4	10
control(RNAi)	2.7 ± 1.2	2.5 ± 1.4	10
ced-1(RNAi)	20.2 ± 3.4	0.3 ± 0.5	10
rab-5(RNAi)	12.3 ± 2.1	1.4 ± 1.2	10
rab-7(RNAi)	31.7 ± 6.5	29.0 ± 3.1	10
sand-1(ok1963)	12.7 ± 2.1	11.4 ± 4.4	10
vps-39(RNAi)	17.1 ± 2.7	12.0 ± 4.9	10

Table S1c. Phagosomes are not arrested at the DYN-1(+) stage.

Genotype	Corpse Number	Fluorescent Halos	*n*
vfEx123 [P_{ced-1}::yfp::dyn-1]	1.8 ± 0.7	1.1 ± 0.5	10
ced-1(RNAi); vfEx123 [P_{ced-1}::yfp::dyn-1]	18.7 ± 1.8	0	10
rab-7(RNAi); vfEx123 [P_{ced-1}::yfp::dyn-1]	28.3 ± 5.5	1.1 ± 0.6	10
sand-1(ok1963); vfEx123 [P_{ced-1}::yfp::dyn-1]	13.0 ± 3.0	1.4 ± 1.0	10
vps-39(RNAi); vfEx123 [P_{ced-1}::yfp::dyn-1]	18.1 ± 3.2	1.6 ± 0.8	10

Table S1d. Phagosomes are arrested at the RAB-5(+), FYVE(+) stage.

Genotype	Corpse Number	Fluorescent Halos	*n*
opEx1314 [P_{ced-1}::yfp::rab-5]	1.7 ± 0.7	1.3 ± 0.9	30
ced-1(RNAi); opEx1314 [P_{ced-1}::yfp::rab-5]	14.2 ± 2.3	0.1 ± 0.3	10
rab-7(RNAi); opEx1314 [P_{ced-1}::yfp::rab-5]	12.2 ± 2.6	9.3 ± 2.0	10
sand-1(ok1963); opEx1314 [P_{ced-1}::yfp::rab-5]	13.7 ± 2.6	10.3 ± 3.8	25
ccz-1(RNAi); opEx1314 [P_{ced-1}::yfp::rab-5]	10.8 ± 1.9	7.1 ± 1.6	10
ccz-1(ok2128); opEx1314 [P_{ced-1}::yfp::rab-5]	13.0 ± 4.0	9.2 ± 2.5	23
vps-39(RNAi); opEx1314 [P_{ced-1}::yfp::rab-5]	13.3 ± 2.5	1.9 ± 1.2	10
opEx1313 [P_{ced-1}::yfp::rab-7]	1.8 ± 0.7	3.1 ± 1.5	20
ced-1(RNAi); opEx1313 [P_{ced-1}::yfp::rab-7]	14.9 ± 2.1	0.4 ± 0.7	10
sand-1(ok1963); opEx1313 [P_{ced-1}::yfp::rab-7]	11.3 ± 2.6	0.1 ± 4.8	21
ccz-1(RNAi); opEx1314 [P_{ced-1}::yfp::rab-5]	11.8 ± 1.8	0.6 ± 1.1	10
ccz-1(ok2128); opEx1314 [P_{ced-1}::yfp::rab-5]	14.8 ± 3.2	0.7 ± 0.4	5
vps-39(RNAi); opEx1313 [P_{ced-1}::yfp::rab-7]	17.0 ± 3.4	19.9 ± 4.8	10
opIs334 [P_{ced-1}::yfp::2xFYVE]	2.5 ± 0.8	2.6 ± 1.4	10
ced-1(RNAi); opIs334 [P_{ced-1}::yfp::2xFYVE]	17.5 ± 2.2	0	10
vps-34(RNAi); opIs334 [P_{ced-1}::yfp::2xFYVE]	13.9 ± 2.8	0.8 ± 0.9	10
rab-5(RNAi); opIs334 [P_{ced-1}::yfp::2xFYVE]	15.3 ± 1.6	0.4 ± 0.5	10
rab-7(RNAi); opIs334 [P_{ced-1}::yfp::2xFYVE]	30.2 ± 8.0	15.1 ± 2.5	10
sand-1(RNAi); opIs334 [P_{ced-1}::yfp::2xFYVE]	16.9 ± 2.1	26.7 ± 4.4	15
vps-39(RNAi); opIs334 [P_{ced-1}::yfp::2xFYVE]	19.2 ± 4.4	5.3 ± 4.4	10

Table S1e. Phagosomes do not acquire LMP-1 in *sand-1(ok1963)* worms

vfEx161 [P_{ced-1}::lmp-1::yfp]	1.9 ± 0.7	2.3 ± 1.6	10
ced-1(RNAi); vfEx161 [P_{ced-1}::lmp-1::yfp]	14.8 ± 2.3	0.1 ± 0.3	10
rab-7(RNAi); vfEx161 [P_{ced-1}::lmp-1::yfp]	17.4 ± 4.2	0.3 ± 0.7	10
sand-1(RNAi); vfEx161 [P_{ced-1}::lmp-1::yfp]	15.6 ± 3.3	0.1 ± 0.4	8
vps-39(RNAi); vfEx161 [P_{ced-1}::lmp-1::yfp]	14.0 ± 2.5	0.2 ± 0.4	10

Table S1f. Recruitment of SAND-1 to phagosomes is normal is *vps-39(lf)* worms

vfIs3 [P_{ced-1}::yfp::sand-1]	2.2 ± 0.8	1.1 ± 1.0	10
sand-1(ok1964); vfIs3 [P_{ced-1}::yfp::sand-1]	1.4 ± 0.8	NA	10
rab-5(RNAi); vfIs3 [P_{ced-1}::yfp::sand-1]	13.4 ± 2.5	0.4 ± 0.7	10
rab-7(RNAi); vfIs3 [P_{ced-1}::yfp::sand-1]	19.9 ± 4.5	1.8 ± 0.8	10
vps-39(RNAi); vfIs3 [P_{ced-1}::yfp::sand-1]	15.3 ± 2.2	0.9 ± 1.0	10

Supplemental Online Methods

Identification of two evolutionarily conserved genes regulating processing of engulfed apoptotic cells

Jason M. Kinchen and Kodi S. Ravichandran

Nematode strains and reagents

Nematode strains were cultivated as previously described[35]. Alleles used were as follows: *LGI: ced-1(e1735); LGIII: ced-6(n1813), LGIV: sand-1(ok1963), opIs110[P_{lim-7}::yfp::act-5]; LGV: ccz-1(ok2128). opEx1304 [P_{ced-1}::yfp::rab-5; unc-119(+)] and opEx1303 [P_{ced-1}::yfp::rab-7; unc-119(+)]* are extrachromosomal arrays and were described previously[13]; *vfEx152* and *vfEx186* were generated by were generated by micoinjection of P_{ced-1}*::yfp::sand-1* or P_{ced-1}*::yfp::rab-5*, P_{ced-1}*::cfp::rab-7* and P_{ced-1}*::mCherry::sand-1* into *unc-69(e587)* worms as described[13]; *vfEx152* was integrated by brief exposure to UV to generate *vfIs3*, which was then backcrossed at least 5x to wild-type.

Reagents used in this study were AlexaFluor 488 rabbit anti-GFP, Lysotracker Red, acridine orange (Invitrogen), anti-FLAG M2 HRP conjugate (Sigma), anti-HA (clone F-7) HRP conjugate and anti-GFP (clone B2) HRP conjugate (Santa Cruz) and anti-RabGDI (Invitrogen). Mammalian Rab7 expression constructs were a gift from Dr. Angela Wandinger-Ness[36].

RNAi studies

Feeding RNAi in *C. elegans* was performed as described[37] with the following modifications. NGM-agarose plates containing 2-10mM IPTG ("RNAi plates") and 100μg/mL carbenicillin were inoculated with ~300μL of appropriate bacterial cultures (transformed with constructs for generation of double stranded RNA under the control of

the T7 promoter) and incubated for 8-12h before addition of worms. Between 30 and 60 synchronized L1 stage worms were placed on each RNAi plate and left for 72h at 20°C. Worms fed with HT115(DH3) bacteria transformed with the original L4440 RNAi vector containing no insert were used as a reference strain.

DIC and fluorescence microscopy (nematode)

Worms were placed on 2% agarose pads in M9, anaesthetized with 3-5mM levamisole (Sigma) and mounted under a cover slip for observation using a Zeiss Axiovert 200 microscope equipped with DIC (Nomarski) optics and standard epifluorescence with filter sets appropriate for visualization of YFP, CFP. For localization studies with mCherry::SAND-1, worms were imaged using an AxioImager Z2 with epifluorescence and filtersets for imaging YFP, CFP and mCherry then deconvolved using the Fast Iterative method in AxioImager.

Where appropriate, images were pseudo-colored in Adobe Photoshop CS3. Staining of worms with Acridine Orange or Lysotracker Red (Invitrogen) were performed as previously described[11, 13]. Briefly, gonads were dissected in PBS supplemented with ~1mM Lysotracker Red, then incubated in the dark for 2 minutes prior to observation.

To score apoptotic corpses in the hermaphrodite germ line, clean worms were synchronized by picking hermaphrodites at the L4 larval stage (Christmas tree vulva). These worms were incubated for 24h at 20°C then scored for persistent cell corpses and fluorescent halos where appropriate. For most animals only one gonadal arm was scored, as the other arm was usually concealed by the intestine.

Accumulation of corpses can be also scored in the pharynx of the worm. Although *sand-1* deficient worms accumulated exogenous lysosomes in the pharynx, which resemble apoptotic bodies but appear more condensed under DIC optics[21], these structures

remained in *sand-1(ok1963); ced-3(n717)* double mutants (data not shown), confirming they likely arose independent of cell death. Thus, we chose to focus our studies on the adult hermaphrodite gonad.

Immunofluorescence analyses in mammalian cells

Cells were incubated overnight in Lipofectamine 2000 as previously described[38], washed and incubated in DMEM + 10% serum ~8h before engulfment assay was conducted. For siRNA experiments, cells were transfected using Amaxa program U-30 and Kit R for NIH/3T3 cells (Amaxa, Germany) with an siRNA SMARTpool containing 4 siRNAs targeting mouse *mon1a* (Dharmacon cat # M-049528-01), *mon1b* (M-055500-01) or a noncoding SMARTpool (Dharmacon cat # D-001206-13) using 1.2 µg of total siRNA (0.3 µg of each individual siRNA) as previously described[13, 39], then incubated 48h to recover. Images were acquired using a Zeiss 510-UV laser scanning confocal microscope with 405, 488, 543, and 633nm lasers (Zeiss AG, Germany).

Apoptotic thymocytes were generated as previously described[13, 40]; apoptotic thymocytes (5×10^5 cells per condition) were added to NIH/3T3 cells in 4-well Labtek II culture chambers followed by a brief centrifugation to pellet cells onto the slide. Thymocytes were allowed to be engulfed for 30 minutes; unbound apoptotic thymocytes were gently washed off with DMEM + 10% FBS, and then subsequently incubated for 2h. For Lysotracker staining, cells were incubated with apoptotic cells in DMEM + 10% FBS containing 1/10,000 dilution of Lysotracker Red. Cells were then fixed with 3% paraformaldehyde (Sigma) in PBS for 30 minutes, permeabilized with 0.1% Triton X-100 (Sigma) and blocked with 5% milk that had been clarified by high speed centrifugation. Antibody staining was then done as previously described[38].

Apoptotic thymocytes were used for acidification experiments primarily due to their small size, which results in fast acidification. SCI cells were used for phagocytosis assay

because their large size (relative to thymocytes) leads to better discrimination of minor defects in uptake, which would otherwise be invisible and could potentially influence degradation.

Generation of transgenic nematodes

unc-69(e587) mutant worms were injected with either a *Pced-1::yfp::sand-1* or a *Pced-1::yfp::MON1a* construct as previously described[11, 13]. For *sand-1* constructs, genomic coding sequences were used. For MON1a, a cDNA obtained from Open Biosystems was used. All constructs were sequenced to verify fidelity.

Yeast two and three-hybrid analyses

S. cerevisiae strain HF7c (His^-, Trp^-, Leu^-, Met^-) was used to screen for protein:protein interactions between indicated constructs cloned either into pVP16 (containing the VP16 transactivation domain) or pGBT9 (containing the GAL4 DNA-binding domain). For yeast three-hybrid analyses, pBridge vector (Clontech), which allows co-expression of GAL4-DB and NLS-targeted constructs, was used in place of pGBT9. A positive protein:protein interaction in the assay was defined as growth on selective Dropout (DO) plates [Trp^-, Leu^-, His^- (or Met^- for yeast three-hybrid) with 1mM 3-amino-1,2,4-triazole (3AT)]; growth on the appropriate nonselective plate (in the presence of His) was used as a viability control.

Immunoprecipitations

293T cells were transiently transfected with ~2µg each of the appropriate constructs. After ~18h, cells were lysed (in 1% Triton X-100, 50mM Tris and 150mM NaCl) and immunoprecipitated using anti-FLAG (clone M2, Sigma), anti-HA (clone F7, Santa Cruz) or anti-GFP (B-2, Santa Cruz) antibody directly coupled to agarose or sepharose.

For RabGDI assay, MON1a and CCZ1 were transiently transfected into 293T cells; after ~18h, cells were processed as above to immunoprecipitate ^{FLAG}MON1a and ^{FLAG}CCZ1. Proteins were then eluted from the anti-FLAG agarose using FLAG peptide (Sigma). Separately, 293T cells were transiently transfected with ^{HA}Rab7; after ~18h, cells were lysed and Rab7 immunoprecipitated using anti-HA sepharose (Santa Cruz). Rab7 was stripped of nucleotide using EDTA, then re-loaded with GDP in the presence of Mg^{2+} before incubation with purified RabGDI (Jena Bioscience), and aliquoted into separate tubes. Eluted ^{FLAG}MON1a and ^{FLAG}CCZ1 were then added to designated tubes (both individually or together) and incubated with HARab7:RabGDI complex for ~1hr at 4˚C, washed 3x in TBS + 0.1% Triton X-100 + 5% glycerol + 5mM $MgCl_2$, and analyzed by immunoblotting. "Negative control" represents eluted protein from mock immunoprecipitation of cells expressing a FLAG peptide from pEBB vector.

Statistics

Student's t test (either unpaired for Figs. 2 and 3 or paired for Fig. 4) were computed using GraphPad Prism. Microsoft Excel was used to make charts for experiments for aesthetic reasons.